ORIGINAL ARTICLE

An experimental study of Lode angle impact on the rock failure procession based on acoustic emission

Hong Yin · Wanchun Zhao · Tingting Wang ·
P. G. Ranjith · Chundi Feng · Wensong Wang

Abstract The laws of acoustic emission (AE) before and during rock failure are different under different stress states. In this article, a new multi-functional true triaxial geophysical (TTG) apparatus was applied to analyze the AE law of sandstone under different stress paths. The results show that (1) with the increase of Lode angle, the tensile fractures in the sandstone increase initially, followed by a decrease. The number of AE decreases initially, followed by an increase, while the average energy of AE signal increases initially, followed by a decrease. (2) During the loading process, the IB values of rock can be divided into wave type, band type and mixed type, which represent crack propagation process driven by external force, self-driving and mixed driving. It can provide a basis for early warning of underground engineering construction disasters. (3) The variation characteristics of RA and AF in rock failure process show the corresponding relationship with IB value. The RA value corresponding to the IB value of band, wave and distribution type distribution mainly concentrated around 0.05, 0.03 and widely distributed, respectively. According to the value of RA, the types of cracks show different characteristics under different driving forces. (4) With the increase of Lode angle, the failure types of rocks change from single oblique fracture ($-30°$) to double-X-type fracture ($10°$), and finally changes to single-X-type fracture when Lode angle is $30°$. The fracture angle of rock decreases initially, followed by an increase with the increase of Lode angle. Therefore, it is important to explore the AE law of rock failure process under different stress states for the early warning of underground engineering construction disasters, and can provide a guidance for the application of human underground space.

H. Yin
Engineering Research Center for Waste Oil Recovery Technology and Equipment, Chongqing Technology and Business University, Chongqing 400067, China
e-mail: yinhgself@sina.com

W. Zhao (✉)
School of Petroleum Engineering, Northeast Petroleum University, Daqing 163318, Heilongjiang, China
e-mail: sdgxwws@163.com

T. Wang (✉)
Electrical Engineering and Information, Northeast Petroleum University, Daqing 163318, Heilongjiang, China
e-mail: wangtingting@nepu.edu.cn

P. G. Ranjith
Deep Earth Energy Laboratory, Department of Civil Engineering, Monash University, Building 60, Melbourne, VIC 3800, Australia

C. Feng · W. Wang
College of Environment and Civil Engineering, Chengdu University of Technology, Chengdu 610059, Sichuan, China

Springer

Article Highlights

- With increasing Lode angle, the number of acoustic emission (AE) signals in rock first decreases then increases, while the average AE energy first increases then decreases.
- The improved b-value (IB) of AE can indicate the crack propagation mode as driven by external force, self-driving, or mixed-driving, providing a basis for early warning of underground construction disasters.
- The fracture angle and failure mode of rocks change with increasing Lode angle, from single oblique to double X-type, and finally to single X-type fractures.

1 Introduction

The failure process of geo-materials, such as sandstone, coal, shale, et al., are accompanied by complex crack propagation. The crack propagation law depend on the micro-component of material and its stress state (Becker et al. 2010; Murphy and Prendergast 2002). Deep rocks are commonly under true triaxial stress conditions ($\sigma_1 \geq \sigma_2 \geq \sigma_3$) because of geological tectonic evolution. Some triaxial compression tests were usually conducted under conventional triaxial stress states to investigate crack propagation process ($\sigma_1 \geq \sigma_2 = \sigma_3$) (Liu and Shao 2018; Walton et al. 2018). However, ignoring the effects of intermediate principal stress (σ_2), it is hard to reflect the failure process of rocks under in-situ stress state. In previous true triaxial experiments, Mogi et al. (1967, 1971) conducted experiments on the effects of intermediate principal stress with the self-developed true triaxial experimental apparatus. Many scholars have Considered the intermediate principal stress (Drucker and Prager 1952; Ewy 1999; Lade 1977), and proposed the true triaxial strength criterion and discussed the applicability of rock strength criteria (You 2009; Benz and Schwab 2008; Danas and Ponte Castañeda 2012). Despite rock strength study considering intermediate principal stress (σ_2), there are few researches focus on the dynamic damage process under different true triaxial stress load paths. In this study, we conducted experiments on changing the Lodes angle under fixed hydrostatic stress. The principal stress directions (i.e., $\sigma_1 \geq \sigma_2 \geq \sigma_3$) are maintained and only their magnitudes are changed within 1/6 of the π-plane. Hence, θ_σ varied from $-30°$ to $+30°$, which is sufficient for investigating the mechanical properties of isotropic materials in the entire π-plane. This loading method exclude the change of the mean stress, and the influence of the change of Lode angle on the damage of sandstone was investigated separately.

AE techniques have been widely applied in structural health monitoring (Lovejoy 2008). When rocks are subjected to loads, micro-cracks start initiating and propagating, and eventually leading to the final failure (Li et al. 2019a; Wang et al. 2020). As one kind of elastic waves, AE propagates through materials to AE sensors (Sagar and Prasad 2012). Fracture type can be inferred by analyzing AE waveforms (Li et al. 2019b). Therefore, these waves have been introducing in test of mechanical properties such as the damage of degree (Carpinteri et al. 2007; Huguet et al. 2002), classification of cracks (Aggelis 2011; Karger-Kocsis and Fejes-Kozma 1994), monitoring of stress concentration areas (Gao and Xing 2018) and location of cracks (Nicolas 2018).

Recently, some studies have applied AE techniques on the true triaxial experiments. For instance, Nicolas et al. (Su et al. 2017) studied the failure behaviors of rocks (*i.e.* granite, sandstone and cement mortars) induced by local dynamic disturbance under true triaxial compression by AE signals. Su et al. analyzed the AE activity during rock burst, and found a 'quiescent period' in the evolution of both AE hits and elastic waveforms on the eve of rock burst. Nasseri et al. conducted experimental research on the AE tests of Fontainebleau sandstone under true triaxial compression combined with micro-CT tomography (Nasseri et al. 2014). Browning et al. compared the cracks evolution of dry sandstone under true triaxial and conventional triaxial compression (Browning et al. 2017a). They found that the intermediate principal stress suppresses the total number of cracks and constraints their growth orientations subnormal to the minimum principal stress. However, in their work, the hydrostatic stress is constant changing, which will affect the destruction morphology of the material. These studies neglect the study of rock failure

processes with different stress paths under the same hydrostatic stress.

To further investigate the influence of different triaxial compression stress conditions on the rock failure process, we studied the influence of Lode angle on AE characteristics of sandstone failure under the hydrostatic stress of 100 MPa by using a multifunctional true triaxial geophysical (TTG) apparatus (Li et al. 2016). The results can provide guidance for monitoring of rock crack propagation and disaster warning in engineering practice under true triaxial stress states. Furthermore, these investigations into rock failure characteristics and AE properties under true triaxial conditions are of paramount importance. They provide essential insights into underground rock stress states and failure mechanisms, playing a critical role in advancing the fields of rock mechanics and geological engineering. This research is also vital for

practical applications, including the design of underground structures and the optimization of resource extraction, highlighting its significance in both scientific research and engineering practice.

2 Experiment procedure

2.1 Experimental apparatus

The multi-functional true triaxial geophysical (TTG) apparatus, as shown in Fig. 1a, can provide load up to 6000 kN in two axial directions, 4000 kN in the third axial direction, and 60 MPa fluid injection pressure. There are two AE load plans (AELP) in this apparatus and each AELP is imbedded four AE sensors. The resonant response of the AE sensors used in the AEPL is around 300 kHz, the AE sensors have good
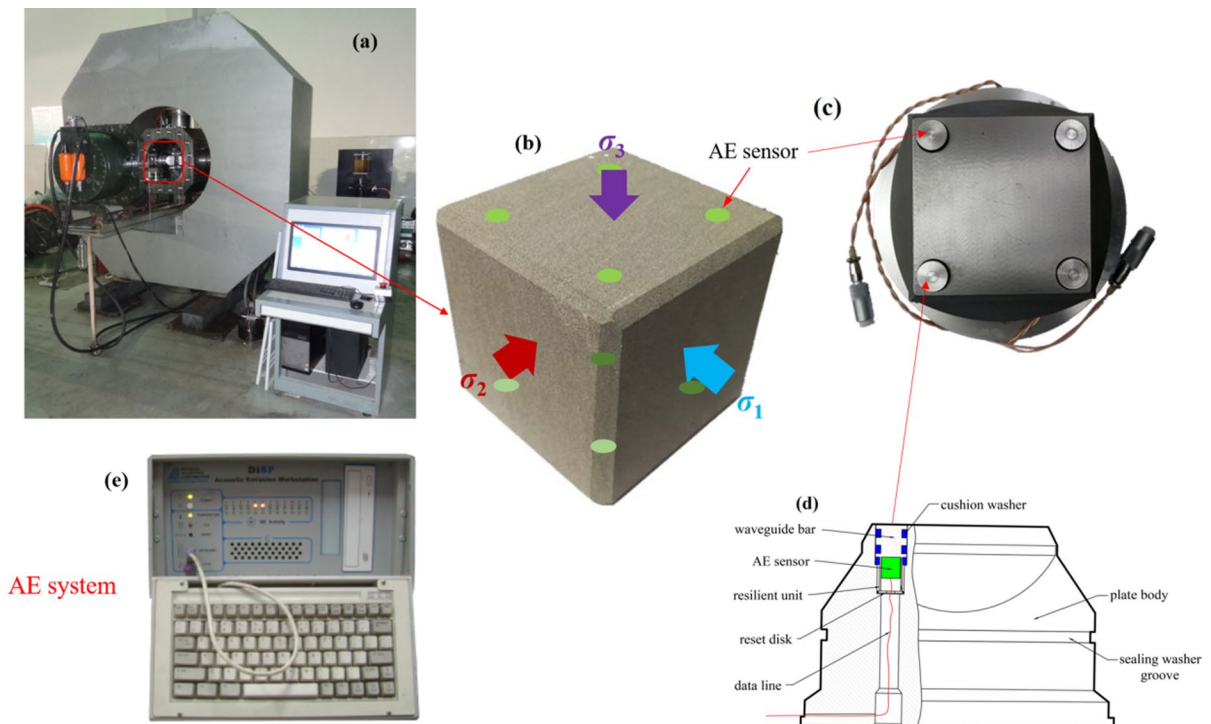

Fig. 1 The test system and specimen. **a** true triaxial equipment test and acoustic AE test equipment **b** Specimen and its loading schematic, **c** image of the AE load plate, **d** internal structure of the AE load plate, **e** the AE system. In **b**, The two loading faces in the direction of the minimum principal stress (σ_3) are the contact faces of the AE sensors, eight green points in figure is the position of the AE sensors, and the opposite face sensors position is completely symmetric

frequency response at the range of 100–900 kHz. To avoid mechanical vibration and ambient noise, the threshold of the AE system was 55 dB. The pre-amplifier gain was locked to 40 dB and the sampling rate was 1 MHz.

2.2 Specimen

Sandstone was collected from Sichuan basin, China. According to international rock mechanics standards, the sandstone is machined into cubic specimens measuring $100 \times 100 \times 100$ mm for three-dimensional servo loading. Although the size of these rock specimens has certain limitations in reflecting the properties of larger-scale rocks, this size is generally accepted in current research on rock mechanical properties. The physical properties of the sandstone are as follows: uniaxial compressive strength is 68.7 MPa, uniaxial tensile strength of Brazilian test is 3.96 MPa, elastic modulus is 4.99 GPa and porosity is 4.78%. The sandstone specimen is shown in Fig. 1b.

2.3 Experimental scheme

Rocks have significant effects of hydrostatic stress. To avoid the effects of hydrostatic stress during rock failure, we studied the effects of stress path in rock failure process under a fixed hydrostatic stress. In this work, the stress cylinder coordinate system was introduced to represent the stress states of rocks. For isotropic materials, the relationship between stress and strain is independent of the coordinate-system's orientation and solely depends on the magnitude of the three principal stresses. As illustrated in Fig. 2, the principal stress space is composed of three orthogonal principal stresses, measured in terms of stress magnitude. When the mean stress (p) is constant, a specific three-dimensional stress path on the π-plane can be characterized by the three principal stresses. The π-plane refers to the plane in the principal stress space whose normal passes through the origin of coordinates and whose external normal is the line of equal inclination $\sigma_1 = \sigma_2 = \sigma_3 = p$. The projections of the three principal stress axes onto this plane are mutually 120° apart. As shown in Fig. 2a, *OO'* represents the normal to the π-plane, with its length equal to the mean stress p; *O'A* represents the deviatoric stress component q of stress *OA*. The Lode angle θ, on the π-plane, is the angle between the *x*-axis and the deviatoric stress component, representing the

relationship between the intermediate principal stress (σ_2) and the maximum and minimum principal stresses (σ_1 and σ_3). The stress at any point can be determined by three parameters: p, q, and θ (for excample, the point S).

Formulas (1)-(7) demonstrate the relationships and mathematical expressions between the mean stress (p), deviatoric stress (q), Lode angle (θ), the intermediate principal stress coefficient (b), and the three principal stresses (σ_1, σ_2 and σ_3).

$$p = \frac{\sigma_1 + \sigma_2 + \sigma_3}{3} \tag{1}$$

$$q = \frac{\sqrt{(\sigma_1 - \sigma_2)^2 + (\sigma_2 - \sigma_3)^2 + (\sigma_3 - \sigma_1)^2}}{\sqrt{2}} \tag{2}$$

$$\tan \theta_\sigma = \frac{2\sigma_2 - \sigma_1 - \sigma_3}{\sqrt{3}(\sigma_1 - \sigma_3)} \tag{3}$$

$$b = \frac{(\sigma_2 - \sigma_3)}{(\sigma_1 - \sigma_3)} = \frac{\sqrt{3} \tan \theta_\sigma + 1}{2} \tag{4}$$

$$\sigma_1 = p + \frac{2}{3q \sin \left(\theta_\sigma + 2\pi/3 \right)} \tag{5}$$

$$\sigma_2 = p + \frac{2}{3q \sin \theta_\sigma} \tag{6}$$

$$\sigma_3 = p + \frac{2}{3q \sin \left(\theta_\sigma - 2\pi/3 \right)} \tag{7}$$

where p, q and θ_σ represent hydrostatic stress, deviatoric stress and lode angle, respectively. σ_1, σ_2, σ_3 represent Maximum, intermediate, and minimum principal stresses, respectively.

In this study, the directions of the three principal stresses remain constant ($\sigma_1 \geq \sigma_2 \geq \sigma_3$). Due to the pronounced isotropic mechanical characteristics of homogeneous sandstone, their magnitudes are altered only within a 1/6 range on the π-plane. The range of variation for θ is from $-30°$ to $+30°$, encompassing typical stress paths. By examining the mechanical properties of sandstone specimens within this range, a comprehensive understanding of the mechanical

Fig. 2 Schematic of Lode angle θ; **a** principal stresses space, **b** π-plane and θ
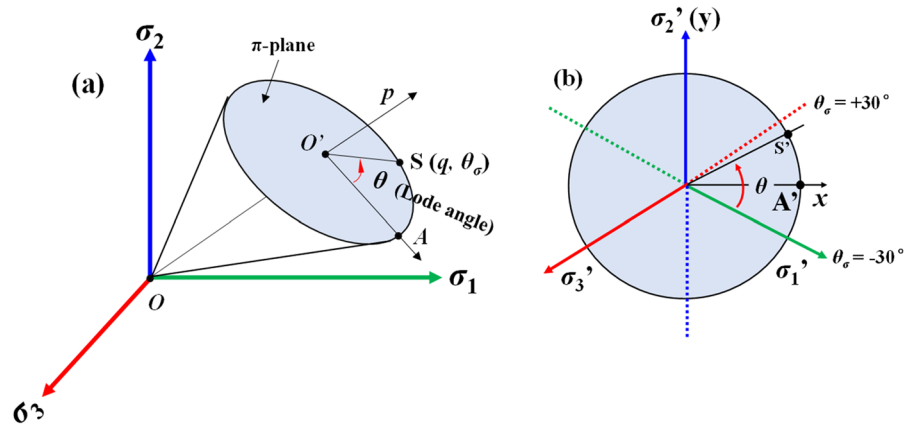
behaviors across the entire π-plane can be achieved. The yielding behaviors of geotechnical materials is essentially considered as a response to the stress state, and using θ as a parameter effectively characterizes the mechanical properties under various three-dimensional stress states. Moreover, when the mean stress p is fixed, the θ and q reflect the magnitude relationship among the three principal stresses on the π-plane. Geometrically, this is manifested as different 3-D stress paths, as shown in Fig. 2b. Therefore, stress state in π plane can be divided into four sections by the Lode angle, as shown in the Table 1.

In this experiment, six different Lode angles were tested under the initial hydrostatic pressure of 100 MPa. The specimen was kept under the predetermined hydrostatic stress of 100 MPa before Lode angle loading test. The specific experimental scheme is displayed in Table 2.

3 Results and discussion

3.1 The distribution of RA and AF values

The AF value and RA values are usually used to evaluate the crack types occurred in geo-material engineering (Aggelis et al. 2012). The classification principle and criterion are shown in Fig. 3. Many scholars have used this principle to classify crack types (Haneef et al. 2013; Li et al. 2018).

According to previous studies (Aggelis 2011), AE signals are shear cracks signals and tensile cracks signals when the AF/RA ratio is small and large (Li et al. 2019a; Wang et al. 2020), respectively. RA

is the growth rate from the initial movement of the stress wave to the maximum peak, as shown in Fig. 3. Thus, the RA value can be used to characterize the rate of energy release during rock rupture. The rate of the AF/RA is determined by the vibration frequency and the energy release rate during crack propagation. Therefore, characteristic of crack propagation in rocks with different Lode angles can be fully reflected by analyzing the distribution law of the AE signal AF-RA.

Figure 4 shows the single distribution of RA and AF produced during the Brazil splitting experiment. We found that the distribution of RA and AF is uniform, but there is a concentrated distribution of a certain frequency in the high frequency area. This may be caused by a specific material under a specific stress state. In order to get more accurate distribution characteristics, we analyzed the distribution statistically. The final statistical result is shown in Fig. 4b. Most region of Fig. 4b are clear and the AE signals of Brazilian splitting are distributed in high frequency region. The RA and AF values of the AE signals are mainly distributed at the range of 0–0.5 and 150–300, respectively. According to the formula ($\omega = 2\pi\, k^{1/2}\, m^{1/2}$), the frequency of the AE waveform is related to the nature of the material and its stress state. Meanwhile, in the Brazilian splitting experiment, most cracks are assumed as tensile cracks. The RA values are always at the range of 0–0.2. Therefore, the minimum frequency of signals is 150 and RA at the range of 0–0.2 can be considered as tensile cracks. The variation of AF at small interval indicates that materials produced crack signals have

Table 1 Relationship between the Lode angles interval and stress states

Lode angle	Stress states
30°	Compression
$30° > \theta > 0°$	Compression-shear
$0° > \theta > -30°$	Tensile-shear
$-30°$	Tensile

Table 2 Stress path of Lode angle tests

Lode angle	Loading rate (kN/s)		
	σ_1	σ_2	σ_3
$-30°$	$+1$	-0.500	-0.500
$-20°$	$+1$	-0.347	-0.653
$-10°$	$+1$	-0.185	-0.815
$+10°$	$+1$	$+0.227$	-1.227
$+20°$	$+1$	$+0.532$	-1.532
$+30°$	$+1$	$+1.000$	-2.000

similar densities and stiffness. There are also some shear cracking signals (high RA and low AF) in Fig. 4. These shear cracks are generated by the local compression at the end of disk in Brazilian splitting experiment.

The distributions of RA-AF under different Lode angles are shown in Fig. 5. The distribution of RA values will appear obvious in high frequency region under different conditions. As a results, the corresponding relationship of AF-RA will also change under different stress paths subsequently. The AF values of AE signal increases with the increase of Lode angle at the range of 0.01–0.1. However, the AF value of AE signal at the range of RA from 1 to 10 decreases with the increase of Lode angle. When the Lode angle is 10°–20° the amount of AE signals increases significantly in the RA range of 0.01–0.1. According to the distribution of AF-RA in Brazil splitting experiment, the tensile failure signals of sandstone is characterized by AF greater than 150 and RA between 0.01 and 0.2. Therefore, it can be inferred that with the increase of Lode angle, the tensile fractures in sandstone increase at the beginning and then decrease.

As shown in Fig. 5, the signals with high AF values clearly show a band distribution. Because the frequency of AE is determined by materials and stress states, the band distribution represents the AE signals produced by the same materials. Rock failure include the collapse of cement and particle breakage. Since most of the cracks in Brazilian splitting experiment are tensile cracks and the probability of particles breakage in Brazilian splitting experiment is relatively small. According to the experimental results of the Brazilian splitting, the AF values of AE during the experiments are greater than 150, as shown in Fig. 4b. Therefore, it is concluded that the band distribution signals are generated by tensile failure of rock cement. There is a certain band distribution at high frequencies, which
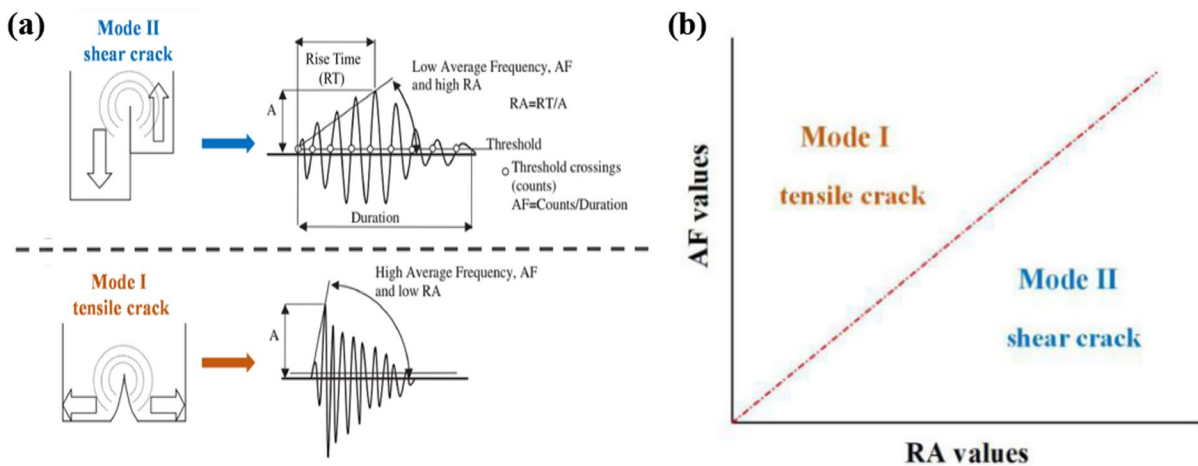
Fig. 3 Crack classification method based on the waveform principle. **a** Waveform principle, **b** crack classification method
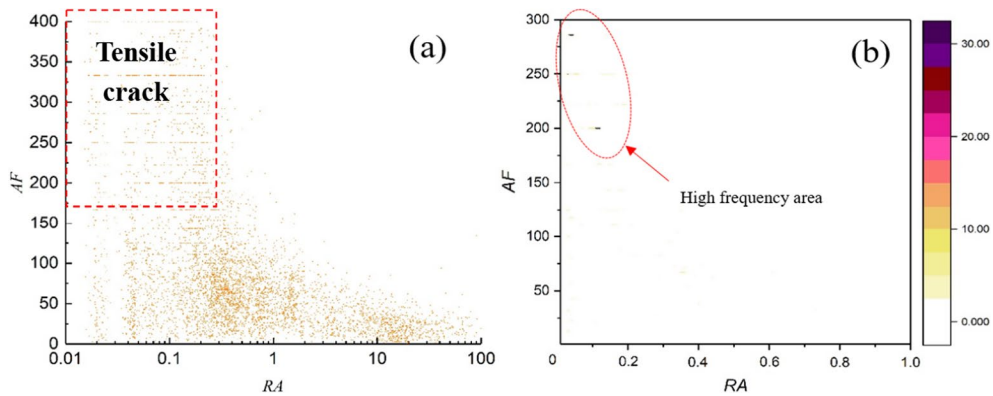
Fig. 4 Distribution of RA and AF in sandstone Brazilian splitting experiment. **a** The RA and AF signals distribution occur during compression, **b** the static result of the RA and AF distribution. Here we define that when more than 2 AE signals appear in the same area, the statistical results will display in that area

may be produced by the rupture of different cement materials in Brazilian splitting experiment.

According to the previous studies, the RA values can reflect the type of cracks, and the energy can reflect the severity of the damage process. Therefore, the occurrence frequency of signals, that is the amount of AE signals at different range of RA values, can reflect the proportion of crack types with high energy. We can get the ratio of energy consumption of different crack types, and infer the main type of fractures that induce rock failure. At the same time, we calculate the average energy (total energy/total number of hits) in each interval of RA.

To compare the AE characteristics under different stress paths intuitively, we set the same value range for the axes as 5000. Therefore, we can compare the change of quantities of AE signal with different Lode angles, as shown in Fig. 6. In triaxial tension state, the number of AE is higher than that of triaxial shear state, which is consistent with the results of previous literature (Browning et al. 2017b). They found that with the increase of σ_2, the amount of AE generated by rock will decrease. However, the maximum Lode angle in their experiments was 0° ($\sigma_1 = 82$ MPa, $\sigma_2 = 43$ MPa, $\sigma_3 = 4$ MPa), which did not reflect all stress path changes. In this experiment, we found that the number of AE signals will increase again with the further increase of σ_2, and up to the triaxial compression state (Lode angle is 30°).

The numbers of AE signal are different under different stress paths. When RA values is around 0.1, the number of AE signal decrease firstly then increase with the increase of Lode angle. The minimum amount occurs when the Lode angle is $-10°$. The Brazilian splitting experiment shows that the RA values less than 0.1 represent extension cracks. However, the type of crack extension represented by different RA values requires further study.

The amount of energy consumed by crack propagation changes with the change of Lode angles. With the increase of Lodes angle, the energy of signals with RA value at the range of 0–1 increased significantly, and reaches a maximum when Lode angles is up to 30°. This indicates that with the increase of RA, the distribution of AE signals is similar in number generated from $-30°$ to 30°, but the energy carried by same type of cracks is quite different. Therefore, to compare the energy changes of cracks release with different Lode angles, the energy carried by average single AE waveform in each RA interval has been calculated. It can be referred that the average energy carried by a single AE waveform also increases with the increase of Lode angle, and reaches a peak value when Lode angle is 20°. The frequency of AE waveform does not increase significantly with the increase of Lode angles, as show in Fig. 5, and the amplitude with different Lode angles does not change significantly, the average amplitude of whole process is around 62 dB as shown in Table 3.
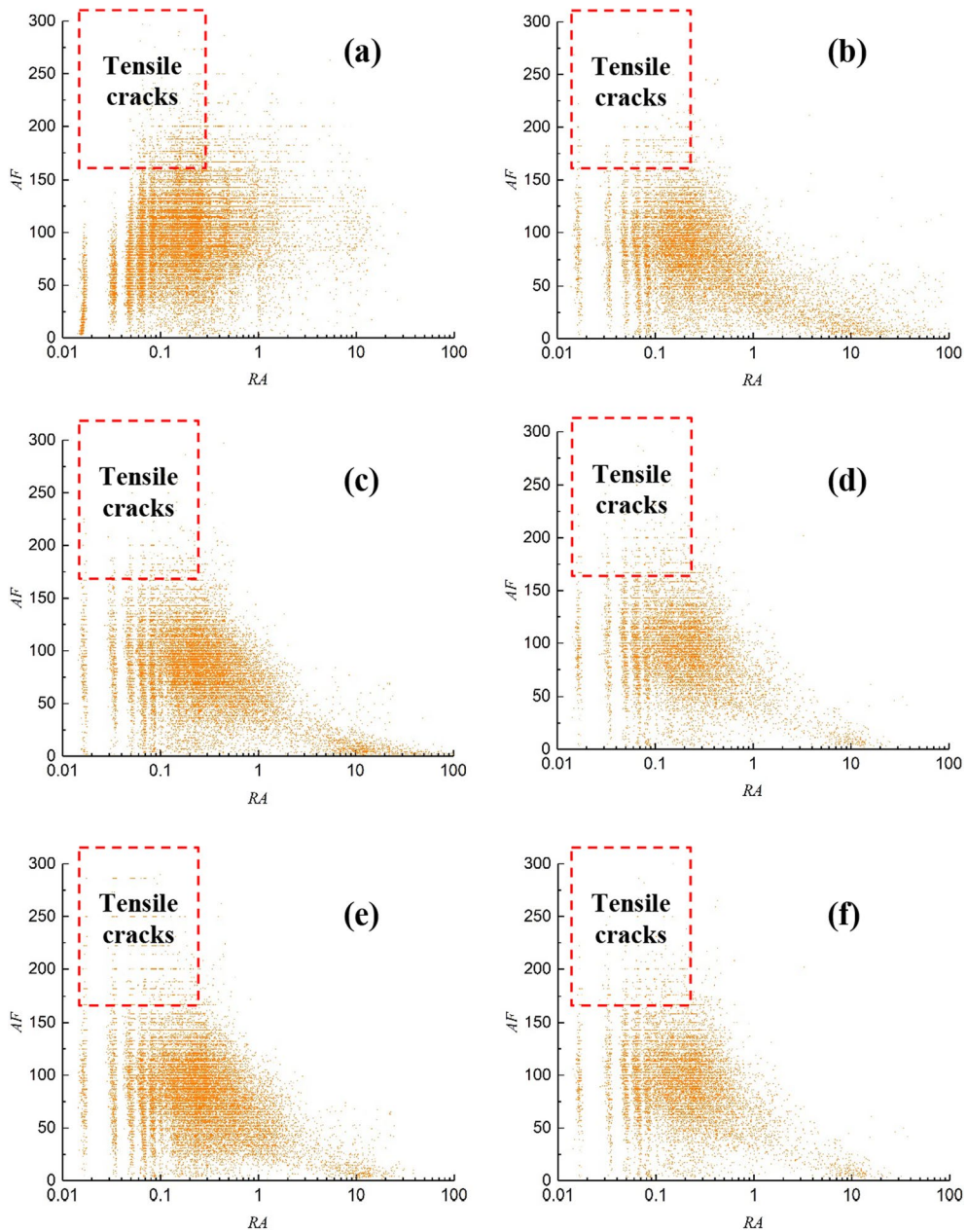
Fig. 5 Relationship between RA and AF values during rock failure in different Lode angle. **a–f** $\theta = -30°$–$30°$

Formula (8) shows that the energy carried by instantaneous vibration is proportional to the square of the amplitude and frequency. The instantaneous vibration energy of the crack propagation does not increase with the increase of the Lode angles. Therefore, the energy increase of a single waveform indicates that the duration of the waveform is longer, hence, with Lode angles increase, the internal crack initiation and propagation time of rocks is longer, that is, the crack length is larger.

$$E = \frac{m}{2} \cdot \omega^2 \cdot a^2 \tag{8}$$
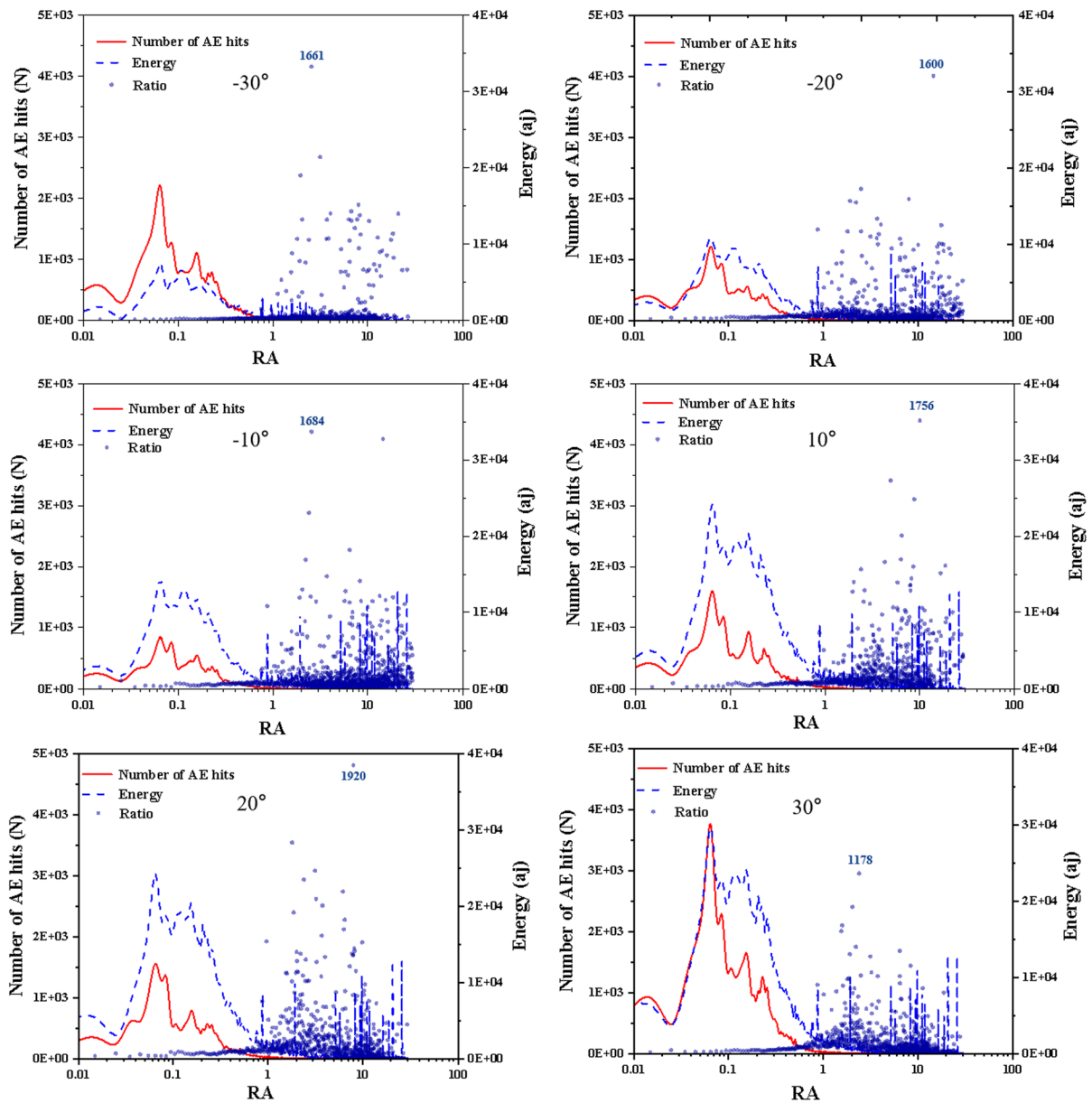
Fig. 6 Statistical values of RA and energy in sandstone under different Lode angle stress paths

where the m, ω and a represents mass, frequency and amplitude, respectively.

With the increase of Lode angles, the crack length also increased. The strain energy is consumed by internal long cracks, which promotes the expansion of main fractures, and result in the decrease of rock strength continuously.

It is similar to the results discussed by Song et al. (2019), with the increase of the ratio of σ_2 and σ_3, the

energy concentrated on the surface of rock fracture increase gradually. The accumulated energy on rock fracture eventually causes the shear scratches on broken section become obvious.

3.2 Crack propagation

Stress paths will significantly influence the direction and proportion of the damage of cement and particles

Table 3 Average amplitude of whole process. (unit: dB)

Lode angle	$-30°$	$-20°$	$-10°$	$0°$	$+10°$	$+20°$	$+30°$
Ave-amp	62.9	62.8	62.9	62.1	62.4	61.9	62.4

in rocks and concrete, thus forming different fracture modes. Some scholars have discovered that waveform features of AE signals are closely related to fracture modes of concrete (Huguet et al. 2002; Aggelis et al. 2011). Different fracture modes produce AE events with different amplitudes and frequencies (Li et al. 2019b). The trend of the improved B-value (IB value) reflects crack size in rocks, and it is a statistical method based on the amplitude of AE signals (Shiotani et al. 1994). A larger IB value indicates that the internal material damage is mainly damage at microscale, and a smaller IB value indicates that the damage is mainly heavy damage. The mathematical principle is expressed as follows:

$$IB = \frac{\log_{10} N(w_1) - \log_{10} N(w_2)}{(\alpha_1 + \alpha_2)\sigma} \tag{9}$$

where $N(w_1)$ and $N(w_2)$ are the numbers of events with an amplitude greater than μ-$\alpha_1\sigma$ and μ-$\alpha_1\sigma$, respectively. In IB value analysis, the number of amplitude is calculated as follows:

$$\int_0^\infty n(a)da = \beta \tag{10}$$

where $n(a)$ is the number of events at da, when the data is fitted to the Gutenberg-Richter equation, the appropriate value of β ranges from 50 to 100 according to the results of the correlation coefficient fitting. A value of β is consider suitable when the log N and AE amplitude fitting similar with a straight line.

In IB value analysis, statistical methods are used to determine the range of AE amplitude, and $N(w_1)$ and $N(w_2)$ are calculated as follows:

$$N(w_1) = N(\mu - \alpha_2\sigma) = \int_{\mu-\alpha_2\sigma}^\infty n(a)da \tag{11}$$

$$N(w_2) = N(\mu + \alpha_1\sigma) = \int_{\mu+\alpha_1\sigma}^\infty n(a)da \tag{12}$$

where μ, σ represent the mean and standard deviation of amplitude, respectively; α_1, α_2 are constants.

According to relevant literature and experience, we set $\beta = 50$, $\alpha_1 = 1$ and $\alpha_2 = 0$.

Figure 7 shows the characteristic of IB value during rock failure. According to previous studies (Rao and Lakshmi 2005), high IB values indicate a set of small AE events which associates with the initiation of micro-cracks and slow expansion of existing cracks. While low IB values indicate macro-crack formation, and rapid crack propagation. As shown in Fig. 7, there are two types of events in the experiments. One is that the IB value fluctuates with the increase of strain, which indicates that with the strain increase, the initiation micro-cracks and the rapid expansion of macro-cracks occur alternatively. The fluctuation IB value means cracks expansion requires constant input of energy from the outside (that is, the strain increases continuously). These cracks expansion is called stable expansion. When the loading stops, the crack also stops expanding. The other type of IB value distribution is a band distribution, which indicates that under a certain strain condition, both the micro-cracks initiation and macro-cracks rapid expansion occur in rocks. Cracks with IB values of band characteristics belong to unstable propagation cracks. These crack propagations do not require continuous external energy input, and the self-storing strain energy provides the energy for crack propagation. These cracks are the main crack propagation types that cause disasters. Therefore, the distribution characteristics of IB value can be used as the early warning signal of underground engineering. Meanwhile, there is a distinct mixed distribution of IB values before rock failure. The mixed distribution is different from the band distribution and fluctuation distribution. It indicates that rock failure process is complex because the complex signals in the process.

According to the different IB value distribution patterns during the loading process, we can judge the damage degree of rocks. At the initial stage of hydrostatic stress loading (0–100 kN), a short strip-like distribution occurs. This stage is the internal skeletal structure adjustment, crack closure and micro-crack propagation during the initial loading. As the hydrostatic stress continues to increase (10–100 kN), the

IB value begins to fluctuate with the increasing of strain, which indicates that the internal crack propagation relies on the externally energy. With the further increase of the hydrostatic stress state of the rock (100–1000 kN), the IB value has two types of distribution at the same time (mixing distribution), which indicates that the cracks generated in the rock in this stage contain spontaneously generated and externally driven cracks.

In the deviatoric stress loading period, the IB value showed a fluctuation distribution at first, then a significant band-like distribution appeared in rock failure. Band-like distribution signals indicate that cracks in rock expand spontaneously and rock is going to failure. The fluctuation distribution at first in deviatoric stress loading, which is similar to the distribution in the hydrostatic stress phase. This similar signal distribution means that the changes in rock at two stages are similar. They are consuming external energy for the adjustment of internal skeletal structural and stress redistribution. The engineering disasters are not likely to occur at this stage.

The crack damage characteristics at different loading stages were analyzed by IB value. The spontaneously expansion cracks mainly occur in the period of the increase of hydrostatic stress and pre-peak stage, and the external drive cracks mainly occur at the initial loading stage of deviatoric stress. The IB value method mainly concentrates on the sequence of crack propagation. The individual signals contain a lot of crack information in their waveforms, which can help us to inverse crack types. Therefore, the nature of individual waveforms needs further investigation. In this article, the distribution of RA and AF values is used to analyze the single waveform signal in sandstone damage.

3.3 RA-AF characteristic in sand rock failure process

In the loading process, the rock will experience different failure stages and produce different cracks. The AE characteristics are different, and then show different IB distribution characteristics in different stages. To further analyze the variation characteristics of RA and AF in different failure stages, the frequency distribution characteristics of RA and AF in AE signals generated at different stages are counted, and the results are shown in Fig. 8. The IB distribution characteristics of rock in different loading stages

are different, and the corresponding RA and AF frequency distribution are also different. In initial loading stage, IB mainly presents bands and fluctuation distribution, and RA values are mainly around 0.04, 0.05 and 0.1. With the increase of load, the distribution frequency of RA value at 0.1 first increases, and then decreases slowly. During the whole loading process, the distribution frequency of RA is mainly at 0.03, 0.05 and 0.1. The peak value of AF distribution frequency distributes at the range of 150–175, which has little change in different rock stages. To further analyze the relationship between the variation characteristics of IB value and the frequency distribution of RA-AF, we analyzed the RA-AF distribution of typical IB value during experiment. The detailed analysis is shown in Fig. 9.

We analyzed the relationship between different IB distributions and RA. When Lode angle is 10° and the strain is at range of 0.8–0.9, as shown in Fig. 9a, the IB value distribution shows a significant fluctuation characteristic. In this stage, the AF value distribution of AE is between 100 and 250, and the maximum value appears around 175. The value of RA is less than 0.5, and its peak value is 0.03, while the number of signals greater than 0.03 is relatively low. This shows that the AE with crack propagation has a smaller RA value when IB value fluctuates. When Lode angle is 20° and the strain is at the range of 0.11–0.12, the IB value distribution shows obvious band distribution characteristics, as shown in Fig. 9b, the corresponding range of AF value is narrower (125–240), and the maximum value appears around 160. It shows that when the IB value of the AE signal shows a band distribution, the RA value of these signals increase. The peak value of RA distribution appears at 0.05, the RA distribution at 0.03 is low, and the proportion of AE at 0.1 is increased.

When Lode angle is −20° and the strain is around 0.4–0.5, the distribution of IB value shows a significant band distribution, as shown in Fig. 9c. The change of AF in AE of rock fracture is similar to the other two types. When the IB value of the AE signal shows a mixed distribution, the rock not only generates large number of signals with low RA values, but also generates large number of signals with RA = 0.1. Mixed distribution of IB value is produced in rock failure. It indicates that there are types of crack damage in rocks, which confirms the conclusion for IB distribution analysis.
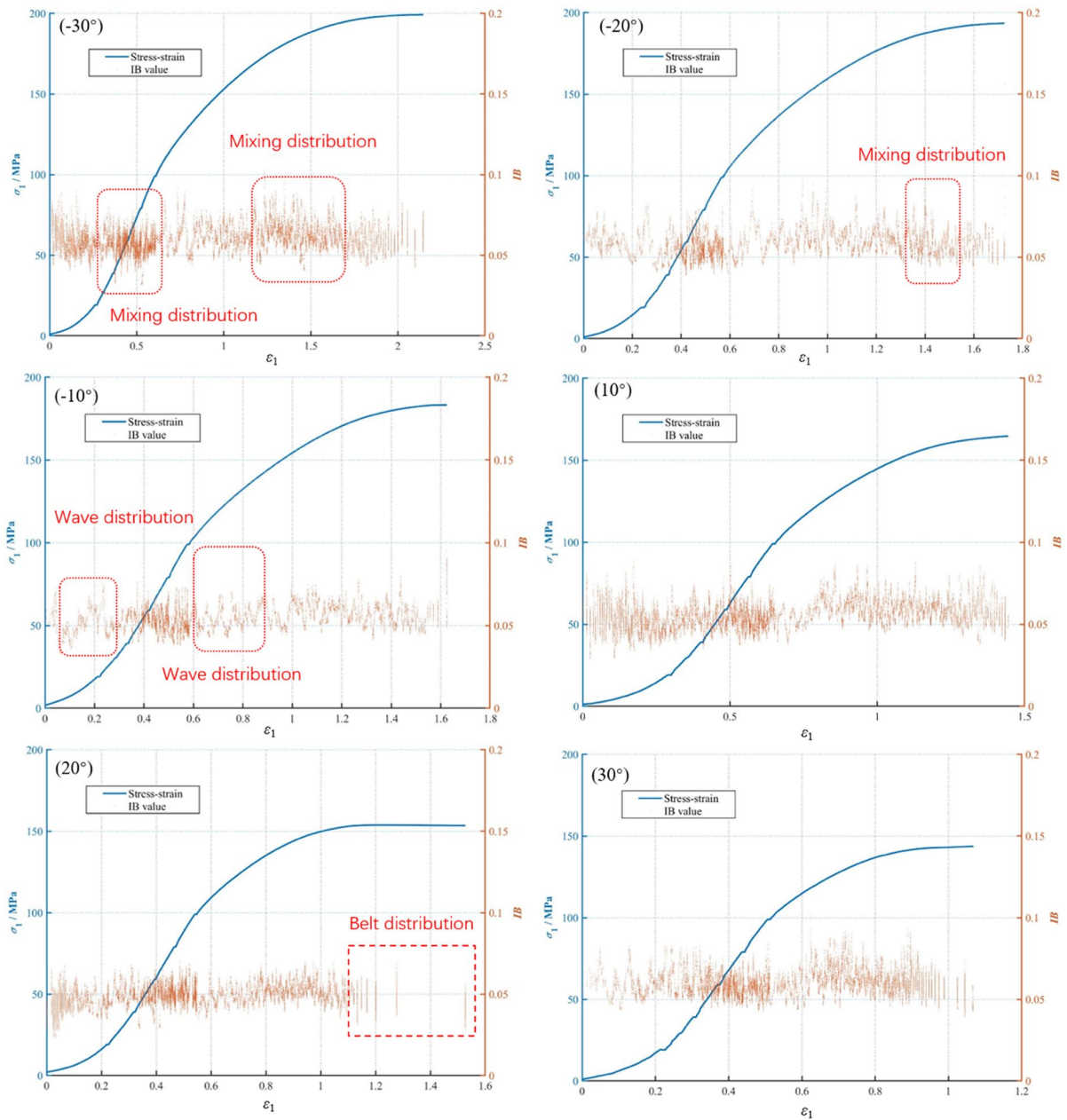
Fig. 7 The corresponding characteristic of IB value and stress–strain

According to the previous analysis, the frequency of AE signal generated by rock fracture is related to rock properties and the stress state. Rocks used in this experiment are homogeneous, so the change of AF is not obvious during the loading process. RA value is related to crack size and propagation state. Therefore, RA can show differences in different stages, and it can be used as an index to monitor rock failure process.
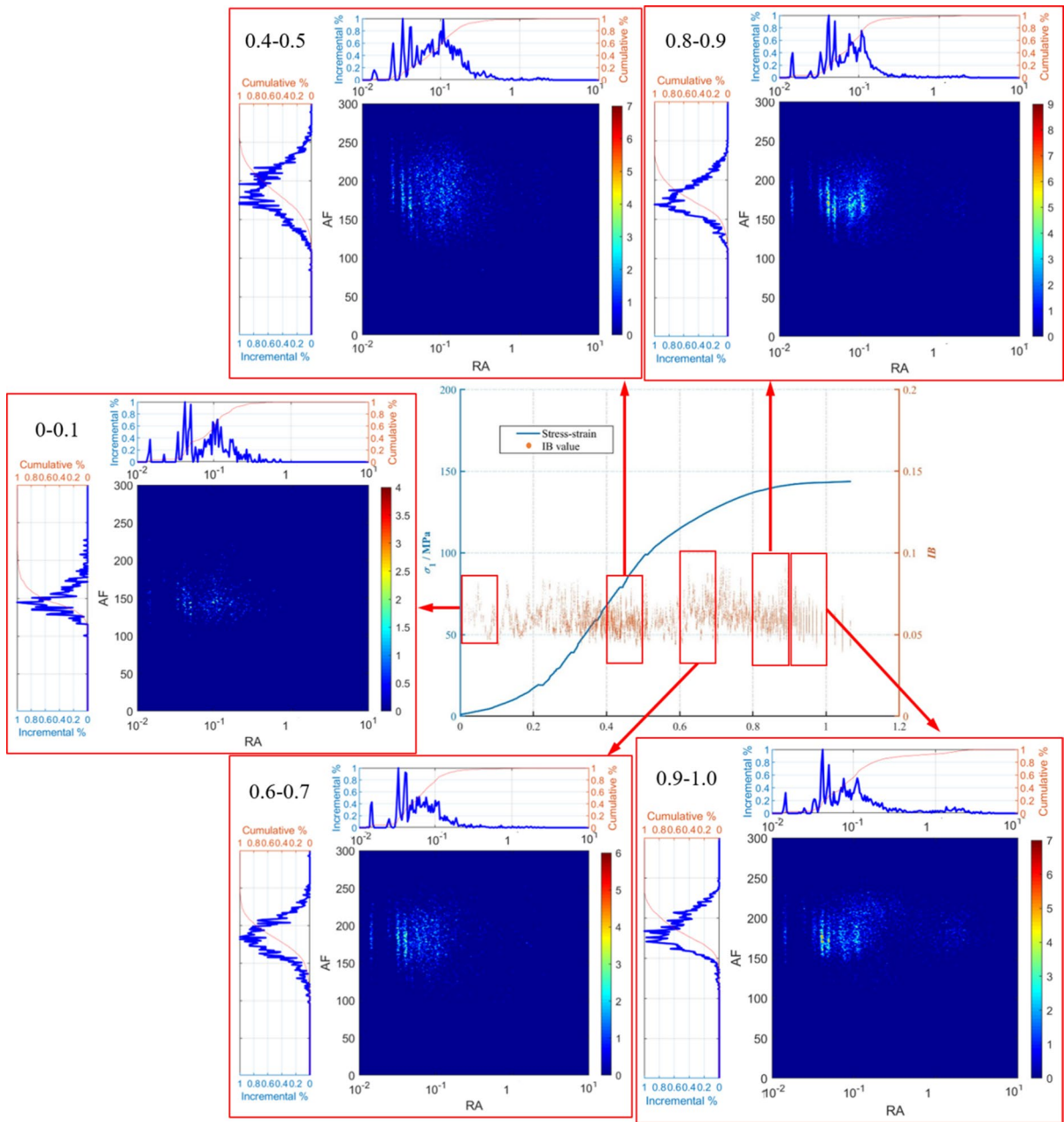
Fig. 8 The corresponding relationship of IB value and RA-AF at different loading stages

3.4 The influence of Lode angle on break angle

Based on the analysts of AE waves, we find that with the change of Lode angle, rock experience different failure stages, and result in different failure models. We have obtained rock fracture morphologies with CT (computed tomography) with different stress paths. The fracture morphology results are shown in Fig. 10.

Previously, studies on rock fracture mainly focus on the way that fix minimum principal stress and increase the intermediate principal stress. It was found
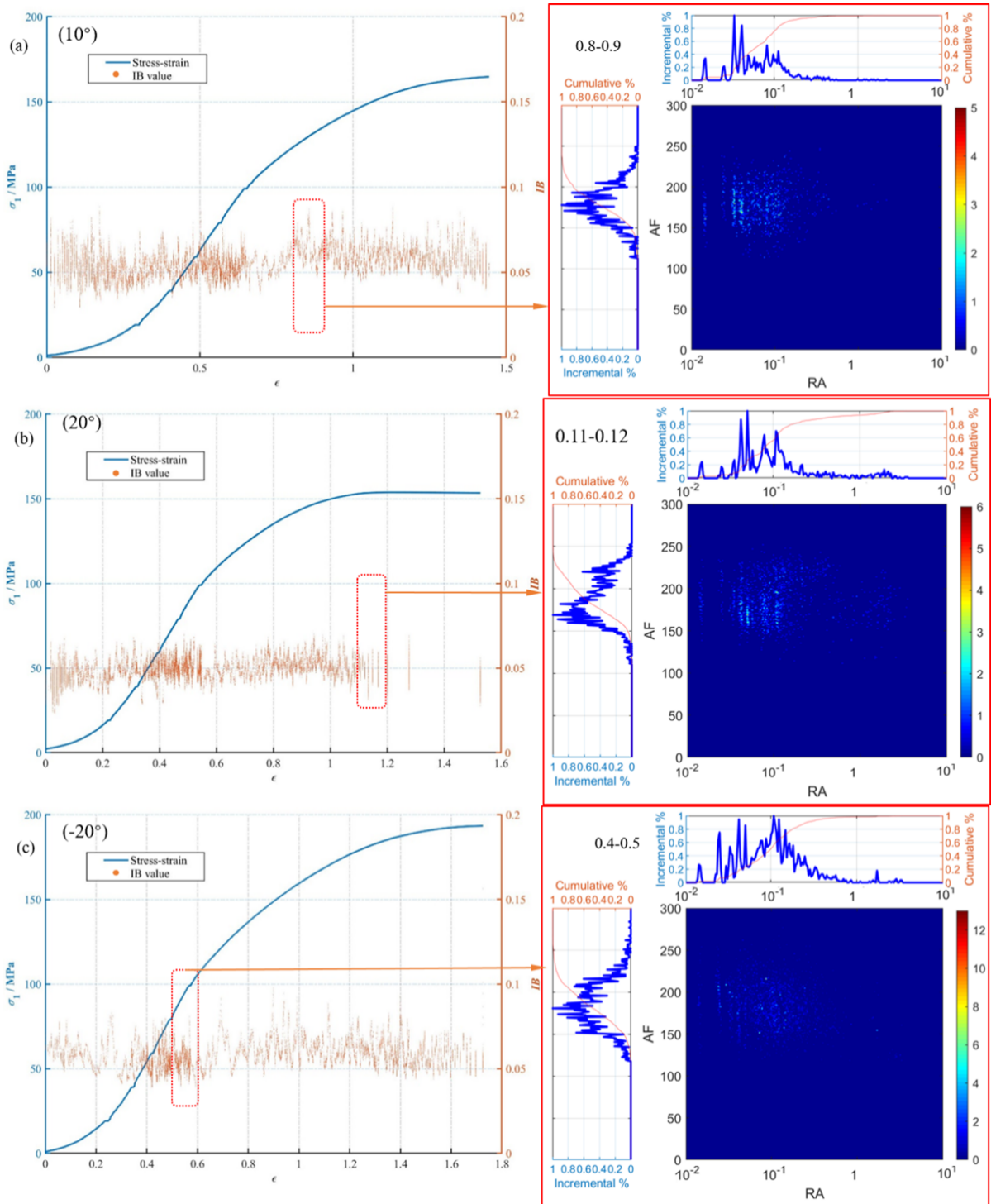
Fig. 9 The corresponding relationship between different IB value and RA-AF

that the fracture angle decrease with the increase of intermediate principal stress (Mogi 2007). However, keeping the minimum principal stress constant, the increasing of intermediate principal stress will also lead to the increase of hydrostatic stress. According to the previous study, the increasing of hydrostatic stress can also cause the decrease of fracture angle (Ma and Haimson 2017). It is hard to separate these two effects. In this work, we kept the hydrostatic stress constant and increased the deviatoric stress until rock failure with different Lode angles (positive relation with intermediate principal stress coefficient). It can be seen from the experimental results that cracks in specimens are not a flat surface. The internal cracks always twist and bend, which results in a great difference between surface crack and internal crack. Therefore, it is inaccurate to determine the fracture patterns only from the specimen surface. We observe the characteristics of rock distortion cracks from the inside, and find that the pattern of rock failure changes as Lode angle changes. When Lode angle is relatively low, the conjugate crack does not penetrate, and rock formed a single inclined fault plane. When Lode angle is $-10°$, the internal cracks appear to X pattern crack. As Lode angle increase, the X pattern crack is becoming increasingly apparent (such as Lode angle is 10°). When Lode angle is 20°, other secondary cracks are generated around the X pattern crack. When Lode angle is 30°, crack pattern changes from double X-type crack to single X-type crack, and large number of second cracks are generated around these X-type crack. These changes in rock failure modes indicate the variation of stress distribution under loading with different Lode angles. According to the above analysis, the rock failure model changes twice with the increase of the Lode angle, rock failure modes transform from an uninterrupted X-type crack to a double X-type crack, which is then converted into a single X-type crack. In our experiments using the Mogi-type rock testing machine, it's crucial to acknowledge the presence of end effects that may impact the fracture patterns at the ends of the rock specimen. Efforts were made to mitigate these effects, such as applying lubricants and adding shims, yet it was not possible to eliminate their influence completely. These end effects primarily affect the fractures at the specimen's ends, with minimal impact on the internal fractures. Since rock fracturing typically initiates from the interior, we can confidently assert
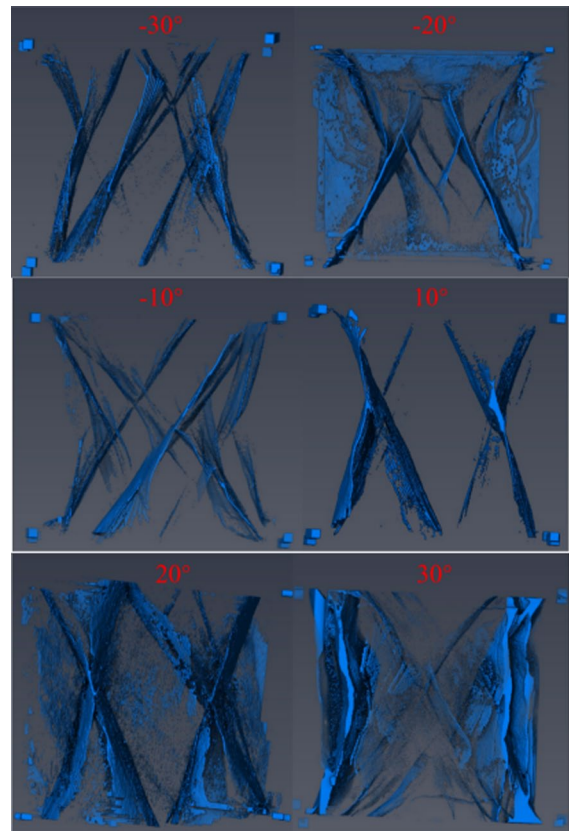

Fig. 10 Fracture types with different stress path

that our experimental results, focusing on these internal fracture patterns, are reliable.

4 Conclusions

In this article, we have investigated the AE law of sandstone under true triaxial stress conditions. The AE characteristics during rock loading under hydrostatic pressure of 100 MPa was studied. Considering the relatively novel experiment and analytical methods, the conclusions of this article are as follows:

(1) The AE characteristics of tensile cracks in the sandstone are obtained by Brazilian splitting experiment. By comparing the distribution characteristics of AF and RA values with different Lode angles, we found that with the increase of Lode angle, the number of tensile fractures

in sandstone increases initially, followed by a decrease. With the increase of Lode angle, the number of AE signals in rock failure decreases initially, followed by increases. While the average energy of AE signals increases initially, followed by decreases.

(2) The change of IB value can be used as the basis to analyze the size of rock crack. The IB value of rock during loading process can be divided into wave type, band type and mixed type, which represent the process of crack propagation driven by external force, self-driving and mixed driving, respectively. It can provide basis for warning of underground construction disasters.

(3) The variation characteristics of RA and AF in rock failure process is related to IB value. The RA value of AE mainly concentrated on 0.05 and fluctuated around 0.03. The RA value of mixed mode distributed widely. According to the value of RA, it can be seen that the types of cracks are different under different driving forces.

(4) With the increase of Lode angle, rock failure mode changes from single fracture ($-30°$) to double-X-type fracture ($10°$), and changes to single-x-type fracture when Lode angle is $30°$. Rock fracture angle initially, followed by increases with the increase of Lode angle.

Declarations

Conflict of interest The authors wish to disclose a potential conflict of interest. Prof. Ranjith, one of the authors, is also the Editor of Geomechanics and Geophysics for Geo-Energy and Geo-Resources. To ensure objectivity and transparency in the review and publication process, Prof. Ranjith was not involved in the editorial review or decision-making process for this manuscript. All other authors declare that there are no additional conflicts of interest regarding the publication of this paper.

References

Aggelis DG (2011) Classification of cracking mode in concrete by acoustic emission parameters. Mech Res Commun 38:153–157. https://doi.org/10.1016/j.mechrescom.2011.03.007

Aggelis DG, Soulioti DV, Sapouridis N, Barkoula NM, Paipetis AS, Matikas TE (2011) Acoustic emission characterization of the fracture process in fibre reinforced concrete. Constr Build Mater 25:4126–4131. https://doi.org/10.1016/j.conbuildmat.2011.04.049

Aggelis DG, Soulioti DV, Barkoula NM, Paipetis AS, Matikas TE (2012) Influence of fiber chemical coating on the acoustic emission behavior of steel fiber reinforced concrete. Cem Concr Compos 34:62–67

Becker D, Cailleau B, Dahm T, Shapiro S, Kaiser D (2010) Stress triggering and stress memory observed from acoustic emission records in a salt mine. Geophys J Int 182:933–948

Benz T, Schwab R (2008) A quantitative comparison of six rock failure criteria. Int J Rock Mech Min Sci 45:1176–1186. https://doi.org/10.1016/j.ijrmms.2008.01.007

Browning J, Meredith PG, Stuart CE, Healy D, Harland S, Mitchell TM (2017a) Acoustic characterization of crack damage evolution in sandstone deformed under conventional and true triaxial loading. J Geophys Res Solid Earth 122:4395–4412. https://doi.org/10.1002/2016JB013646

Browning J, Meredith P, Stuart C, Healy D, Harland S, Mitchell T (2017b) Acoustic characterization of crack damage evolution in sandstone deformed under conventional and true triaxial loading. J Geophys Res: Solid Earth 122:4395–4412. https://doi.org/10.1002/2016JB013646

Carpinteri A, Lacidogna G, Pugno N (2007) Structural damage diagnosis and life-time assessment by acoustic emission monitoring. Eng Fract Mech 74:273–289

Danas K, Ponte Castañeda P (2012) Influence of the Lode parameter and the stress triaxiality on the failure of elasto-plastic porous materials. Int J Solids Struct 49:1325–1342

Drucker DC, Prager W (1952) Soil mechanics and plastic analysis or limit design. Quart Appl Math 10:157–165. https://doi.org/10.1090/qam/48291

Ewy RT (1999) Wellbore-stability predictions by use of a modified lade criterion. Spe Drill Complet 14:85–91. https://doi.org/10.2118/56862-PA

Gao G, Xing Y (2018) Monitoring the evolution of crazing damage in an area under stress concentration via acoustic emission. Int J Precis Eng Manufact 19:561–568

Haneef TK, Kumari K, Mukhopadhyay CK, Rao BP, Jayakumar T (2013) Influence of fly ash and curing on cracking behavior of concrete by acoustic emission technique. Construct Build Mater 44:342–350

Huguet S, Godin N, Gaertner R, Salmon L, Villard D (2002) Use of acoustic emission to identify damage modes in glass fibre reinforced polyester. Composit Sci Technol 62:1433–1444

Karger-Kocsis J, Fejes-Kozma Z (1994) Failure mode and damage zone development in a GMT-PP by acoustic emission and thermography. J Reinf Plasts Composit 13:768–792

Lade PV (1977) Elasto-plastic stress-strain theory for cohesionless soil with curved yield surfaces. Int J Solids Struct 13:1019–1035. https://doi.org/10.1016/0020-7683(77)90073-7

Li M, Yin G, Xu J, Li W, Song Z, Jiang C (2016) A novel true triaxial apparatus to study the geomechanical and fluid flow aspects of energy exploitations in geological formations. Rock Mech Rock Eng 49:4647–4659. https://doi.org/10.1007/s00603-016-1060-7

Li B, Xu L, Shi Y, Chi Y, Liu Q, Li C (2018) Effects of fiber type, volume fraction and aspect ratio on the flexural and acoustic emission behaviors of steel fiber reinforced concrete. Construct Build Mater 181:474–486

Li Y, Long M, Zuo L, Li W, Zhao W (2019a) Brittleness evaluation of coal based on statistical damage and energy evolution theory, Journal of Petroleum Science. Engineering 172:753–763

Li J, Huang J, Niu J, Wan C (2019b) Mesoscopic study on axial compressive damage of steel fiber reinforced lightweight aggregate concrete. Construct Build Mater 196:14–25

Liu Z, Shao J (2018) Strength behavior, creep failure and permeability change of a tight marble under triaxial compression, rock mechanics rock. Engineering 50:1–13

Lovejoy SC (2008) Acoustic emission testing of beams to simulate shm of vintage reinforced concrete deck girder highway bridges. Struct Health Monitor 7(4):329–346

Ma X, Haimson BC (2017) Failure characteristics of two porous sandstones subjected to true triaxial stresses. J Geophys Res 121:6477–6498. https://doi.org/10.1002/2016JB012979

Mogi K (1967) Effect of the intermediate principal stress on rock failure. J Geophys Res 72:5117–5131. https://doi.org/10.1029/JZ072i020p05117

Mogi K (1971) Fracture and flow of rocks under high triaxial compression. J Geophys Res Atmos 76:1255–1269. https://doi.org/10.1029/JZ072i020p05117

Mogi K (2007) Experimental rock mechanics. Taylor and Francis Group, London, UK, p 2007

Murphy BP, Prendergast PJ (2002) The relationship between stress, porosity, and nonlinear damage accumulation in acrylic bone cement. J Biomed Mater Res Part A 59:646–654

Nasseri MHB, Goodfellow SD, Lombos L, Young RP (2014) 3-D transport and acoustic properties of Fontainebleau sandstone during true-triaxial deformation experiments. Int J Rock Mech Min Sci 69:1–18. https://doi.org/10.1016/j.ijrmms.2014.02.014

Nicolas B (2018) Time-resolved tomography using acoustic emissions in the laboratory, and application to sandstone compaction. Geophys J Int 213:2177–2192

Rao MVMS, Lakshmi KJP (2005) Analysis of b-value and improved b-value of acoustic emissions accompanying rock fracture. Curr Sci 89:1577–1582

Sagar RV, Prasad BKR (2012) A review of recent developments in parametric based acoustic emission techniques applied to concrete structures. Nondestruct Test Eval 27:47–68

Shiotani T, Fujii K, Aoki T, Amou K (1994) Evaluation of progressive failure using AE sources and improved b-value on slope model tests. Progress Acoust Emiss 7:529–534

Song Z, Yin G, Ranjith PG, Li M, Huang J, Liu C (2019) Influence of the intermediate principal stress on sandstone failure. Rock Mech Rock Eng 52:3033–3046

Su G, Shi Y, Feng X, Jiang J, Zhang J, Jiang Q (2017) True-triaxial experimental study of the evolutionary features of the acoustic emissions and sounds of rockburst processes. Rock Mech Rock Eng 51:375–389

Walton G, Alejano LR, Arzua J, Markley T (2018) Crack damage parameters and dilatancy of artificially jointed granite samples under triaxial compression, rock mechanics rock. Engineering 51:1637–1656. https://doi.org/10.1007/s00603-018-1433-1

Wang T, Zhang T, Ranjith PG, Li Y, Song Z, Wang S, Zhao W (2020) A new approach to the evaluation of rock mass rupture and brittleness under triaxial stress condition. J Petrol Sci Eng 184:106482

You M (2009) True-triaxial strength criteria for rock. Int J Rock Mech Min Sci 46:115–127. https://doi.org/10.1016/j.ijrmms.2008.05.008

⊴ Springer